Brodogradnja Volume 75, Number 3 (2024) 75307

journal homepage: www.brodogradnja.fsb.hr

Brodogradnja

An International Journal of Naval Architecture and Ocean Engineering for Research and Development

Control method for the ship track and speed in curved channels

He Yanru[1], *Zhao Xingya*[2], *Huang Liwen*[2], *Xu Luping*[2], *Liu Jinlai*[2*]

[1] *School of Marine Engineering, Dalian Maritime University, Dalian 116026, China*
[2] *School of Navigation, Wuhan University of Technology, Wuhan 430063, China*

ARTICLE INFO

Editor-in-Chief: Prof. Nastia Degiuli
Associate Editor: PhD Ivana Martić

Keywords:
Curved channel
Course control
Track control
Speed control

ABSTRACT

Due to natural and external influences in curved channels, ships frequently require adjustments in course and speed, posing challenges for existing control methods. Particularly lacking are speed control methods suitable for curved channel navigation. This study initially developed a three-degree-of-freedom MMG model incorporating external interference. It introduced an OP-PID heading controller merging optimal control strategies with traditional PID, adaptable to both external conditions and ship speed, validated through heading control simulations. The study analysed the ship's speed change process, deriving a mathematical expression for advance distance, and proposed a dichotomy-based speed control method to determine speed change points, addressing differential equations with unknown integrands. To mitigate uncertainty errors like parameter inaccuracies in ship maneuvering models and dynamic environmental disturbances, the study proposed a comprehensive control approach. This approach integrates model predictive control, feedback compensation, segment identification, and an enhanced line-of-sight (LOS) guidance method alongside the OP-PID course controller and dichotomy-based speed control. Simulation experiments in the Dongboliao Channel compared the proposed and existing methods. Results demonstrate the proposed method's capability to handle frequent course and speed adjustments effectively, even under model errors and external interference, showcasing superior track deviation and course control accuracy over existing methods.

1. Introduction

Given the continuous bending, small curvature radius, and restricted navigable width of curved channels, the precise control of the track and speed requires frequent course adjustments. Moreover, the dynamic and intricate nature of these channels necessitates employing techniques like "deceleration before acceleration" to safely manoeuvre vessels through them. Human error or insufficient technical expertise among crew members further complicates navigation and increases the risk of accidents [1]. While existing research has predominantly focused on the impact of curved channel dimensions and current dynamics on navigation safety and regulation, scant attention has been paid to methods for controlling vessel track and speed within these challenging waterways. Therefore, it is imperative to investigate effective track- and speed-control strategies for curved channels.

* Corresponding author.
E-mail address: 15871371582@163.com

http://dx.doi.org/10.21278/brod75307
Submitted 26 April 2024; Accepted 07 July 2024
ISSN 0007-215X; eISSN 1845-5859

Track control in curved channels involves the use of a combination of course controllers and guidance methods to ensure smooth adherence to planned trajectories. Various course-control techniques, such as proportional-integral-derivative (PID) [2], active disturbance rejection [3], sliding mode [4], and nonlinear adaptive heading controllers [5], have been proposed. Although active disturbance rejection and sliding mode control offer comprehensive theoretical frameworks, their practical applications are limited because of the complexity of the navigational environment. In the latest study on track control, a constrained MPC-based ship motion control strategy designed for Z-shaped navigation used a time-driven and event-driven dual-trigger mechanism to control the ship's track, ensuring stable Z-shaped navigation through large waves [6]. The improved Stanley guidance law (ISGL) [7] can evaluate the path curvature in advance and compensate for the desired heading angle to improve the heading angle error and turn an unmanned surface vehicle (USV) in advance. Experimental results show that the ISGL algorithm has a better track-following effect than the traditional integral line-of-sight (ILOS) traditional SGL. On the other hand, the PID control stands out for its simplicity, robustness, reliability, and widespread applicability. To enhance traditional PID control and mitigate course overshoot, researchers have explored the integration of intelligent methods, such as the fuzzy adaptive PID control [8] and neural network-based adaptive PID control [9]. However, these studies typically overlooked the impact of external environmental factors and variations in ship speed on the manoeuvring performance.

In the field of speed control, various methods have been proposed to enhance navigational stability and adaptability. For example, an adaptive inversion error compensation-based speed controller exhibits robustness against unpredictable factors such as wind and waves [10]. Additionally, a collaborative longitudinal speed controller employing model predictive control ensures precise and stable navigation, even during changes in the forward velocity of the ship [11]. Previous studies have explored innovative approaches, such as utilising ship subsidence-based speed control models, to accurately define speed control ranges [12]. Moreover, fuzzy adaptive PID control methods have been found to minimise delays and errors compared with alternative techniques [13]. Furthermore, by leveraging artificial neural networks, researchers have developed joint optimisation decision databases that incorporate factors such as power, draft, pitch angle, and speed to determine the optimal speed for each segment via dynamic programming algorithms [14]. Despite these advancements, many existing speed control methodologies assume instantaneous and arbitrary adjustments to propeller rotation rates, overlooking the gradual changes in ship speed and propeller rotation rate. Bridging the gap between theoretical innovations and practical navigation remains a ripe area for exploration and refinement.

Considering the existing problems in relevant research, this study focuses on the following:

(1) First, the optimal control strategy is combined with the PID to design a heading controller that can adapt to the frequent course and speed alterations of curved channels and complex natural environments.

(2) Considering the practical practice of first decelerating and then accelerating when ships pass a curved channel, the scientific principle of the ship speed shifting process was analysed, and a ship speed control method based on dichotomy was proposed.

(3) Considering that some system errors cannot be eliminated when the theoretical model is used to control an actual ship, a closed-loop track and speed control method was designed based on the theory of model predictive control and feedback compensation to reduce the influence of system errors on the control effect.

2. Ship manoeuvring motion model

2.1 Coordinate system

This study employs both the geodetic coordinate system X-O-Y and the shipboard coordinate system x-o-y, as illustrated in Fig. 1. In the geodetic system, the Y- and X-axes align with the north east, respectively. Conversely, in the shipboard coordinate system, the Y- and X-axes point towards the bow and the starboard side, respectively.

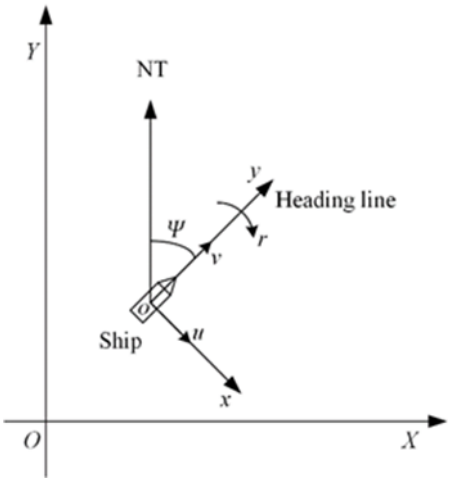

Fig. 1 Coordinate system

Here, Ψ represents the course of the ship, while u and v denote the ship's speed components along the x-axis and y-axis respectively. In addition, r represents the yaw angular speed.

The reasons for using the above coordinate system are as follows:

(1) The positive angle between longitudinal axis Y of the geodetic coordinate system XOY and longitudinal axis y of the shipboard coordinate system xoy is the true course.

(2) A positive angle was consistent with an increase in the direction of the course.

(3) It can be easily connected to the data provided by the AIS and other equipment in the later stages to avoid cumbersome coordinates and angle conversion.

2.2 Mathematical modelling group (MMG) model

In this study, a three-degree-of-freedom MMG model was used to model the ship motion process, as shown in equation (1):

$$\begin{cases} (m+m_y)\dot{v}-(m+m_y)ur = Y_H + Y_P + Y_R + Y_{wind} + Y_{wave} \\ (m+m_x)\dot{u}+(m+m_x)vr = X_H + X_P + X_R + X_{wind} + X_{wave} \\ (I_{ZZ}+J_{ZZ})\dot{r} = N_H + N_R + N_{wave} \end{cases} \tag{1}$$

Variables m, m_x, and m_y correspond to the hull mass, lateral additional mass, and longitudinal additional mass, respectively. The parameters u, v, and r represent the lateral, longitudinal, and yaw angular speeds, respectively. The forces and moments acting on the hull are denoted as X, Y, and N in the lateral, longitudinal, and yaw directions, respectively. H, P, and R represent the hull, propeller, and rudder, respectively. I_{ZZ} and J_{ZZ} denote the moments of inertia and additional inertia, respectively. For a detailed understanding and calculation of these variables, references [15], [16], and [17] should be consulted.

2.3 Model verification

To validate the capability of the constructed MMG model to replicate actual ship motion states, a bulk carrier was chosen as the experimental subject [18], and the detailed parameters are listed in Table 1. The accuracy and suitability of the MMG model were assessed through a series of experiments including hydrostatic cycle experiments, cycle experiments in wind, cycle experiments in waves, cycle experiments in currents, and zigzag manoeuvring experiments.

Table 1 Experimental ship parameters

Parameter type	Ship data
Length	225 m
Breadth	32.5 m
Draft	14.5 m
Displacement	90000×10^3 kg
Maximum rudder angle	35°
Propeller diameter	6.8 m
Pitch	4.738 m

2.3.1 Cycle experiment in still water

The initial course and speed of the ship were set as 000° and 5.4 m/s, respectively. Hard starboard cycle experiments were conducted in still water, as shown in Fig. 2. The turning advance and transverse distances are 3.49 times and 1.92 times in length, respectively. Fig. 3 shows the actual circle data in the still water of the experimental ship listed in Table 1. It can be seen that there is a small difference between Figs. 2 and 3 in cycle diameter, the advance, and the transverse.

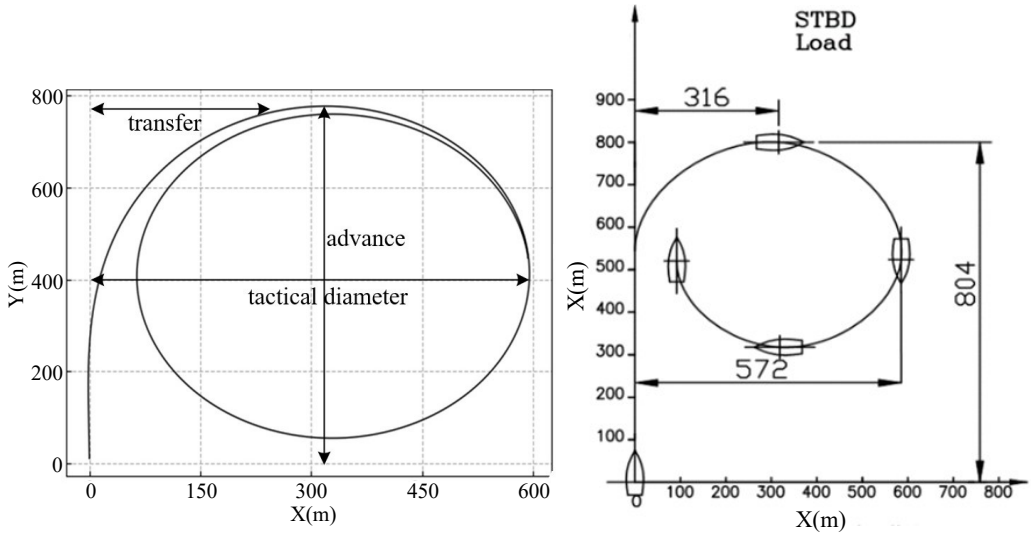

(a) Hard starboard cycle in still water (MMG model) (b) Hard starboard cycle in still water (real ship)

Fig. 2 Cycle experiment in still water

A comparison of the simulation data in Fig. 2(a) with the real ship data in Fig. 2(b) shows that the advance, transfer, and tactical diameters of the MMG model cycle experiment were 782, 345, and 593 m, respectively. The advance, transfer, and tactical diameters of the actual ship were 804, 316, and 572 m, respectively. The parameter errors for each cycle were 2.8%, 9.1%, and 3.6%, respectively. Although there are some errors in the results, they are still within a reasonable range and can meet the engineering requirements. Thus, the accuracy of the MMG model was verified.

2.3.2 Cycle experiment under environmental disturbance

Considering actual sailing, the ship must encounter the influence of wind and current. In this study, a cycle experiment was conducted under environmental disturbances. The simulation conditions were as follows: ship speed of 10.5 knots and a hard starboard. When the wind speed was 4 m/s, the wind direction angle was 000° and the current velocity and direction were 1 m/s and 045°, respectively. The results are shown in Fig. 3.

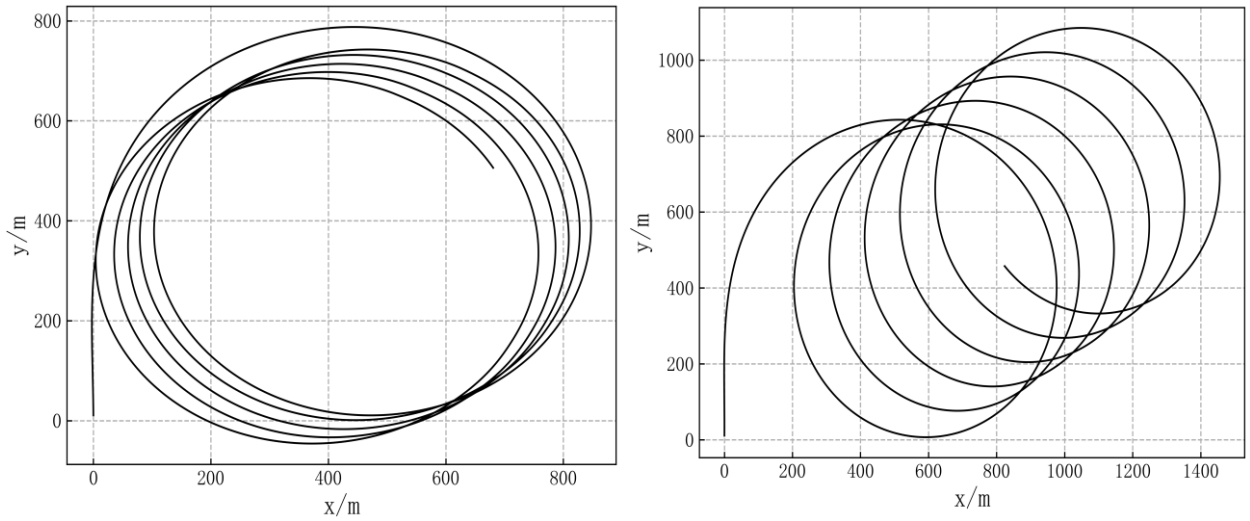

(a) Cycle experiment under wind (b) Cycle experiment under currents

Fig. 3 Cycle experiment under environmental disturbances

The experimental results were compared with those of a wind tunnel experiment conducted by Yang Y. In comparison, there is a small gap between this study and other studies.

2.3.3 Zigzag experiment

The initial course and speed of the ship were set as 000° and 5.4 m/s, respectively. The rotational rate of the propeller was 70 rpm. Zigzag experiments of 10°/10° and 20°/20° were carried out, and the results are shown in Figs. 4 and 5.

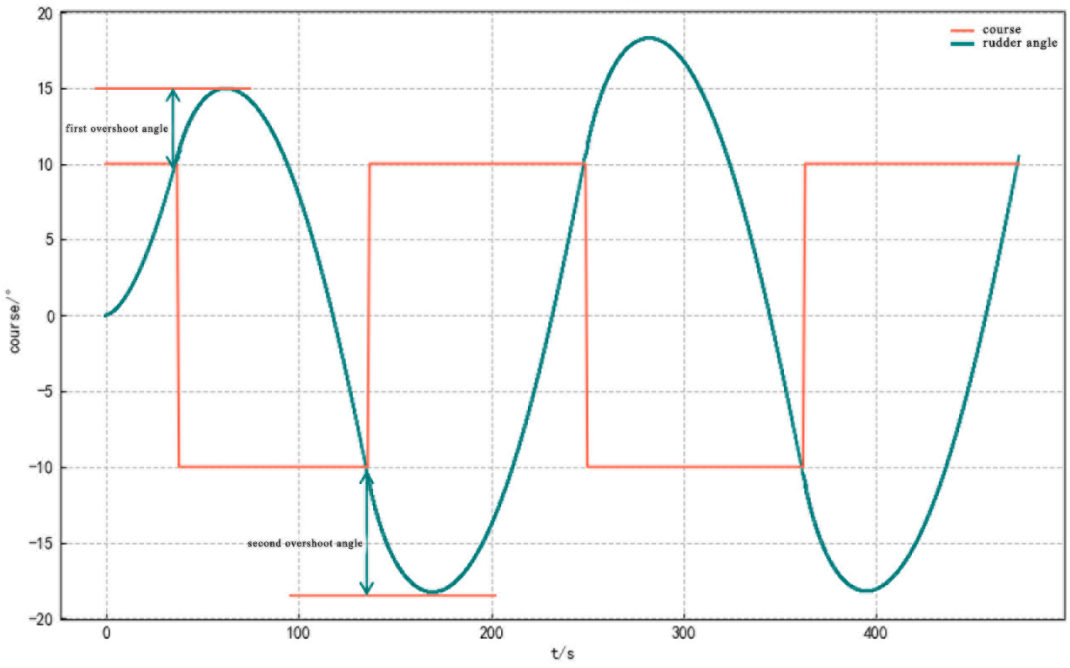

Fig. 4 Zigzag experiment of 10°/10°.

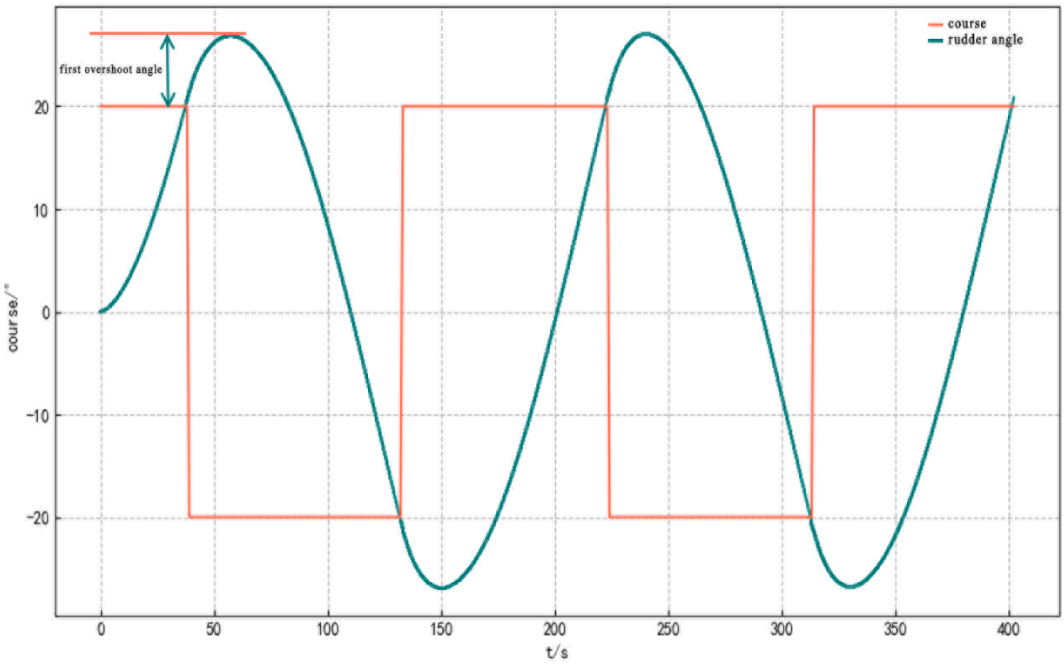

Fig. 5 Zigzag experiment of 20°/20°

In the 10°/10° zigzag experiment, L/V=41.67 s, and the transcendence of the first overshoot angle and the second overshoot angle are 4.9° and 8.3°, respectively. In accordance with the provisions of the International Maritime Organization, when $L/V \geqslant 30$ s, the first overshoot angle of 10°/10° zigzag experiment should be less than 20 degrees, and the second overshoot angle should be less than 40 degrees.

In the 20°/20° zigzag experiment, L/V=41.67 s, and the transcendence of the first overshoot angle is 8.5°. According to the provisions of the International Maritime Organization, the first overshoot angle in the 20°/20° zigzag experiment should be less than 25°. The zigzag experimental results of the constructed MMG model fully complied with the relevant regulations of the International Maritime Organization.

3. Design and simulation of a ship course controller under variable speed

3.1 PID course autopilot

Fig. 6 shows the core schematic of the automated rudder system using the PID control for course regulation. The deviation between the actual course $\Psi(t)$ and the desired course $\Psi r(t)$ is represented as $e(t) = \Psi(t) - \Psi_r(t)$. By employing a linear combination of proportional (K_p), integral (K_i), and differential (K_d) coefficients, the system computes the rudder angle $\delta(t)$ output. This angle is constrained within [-35°, 35°] to effectively steer the ship's course [17].

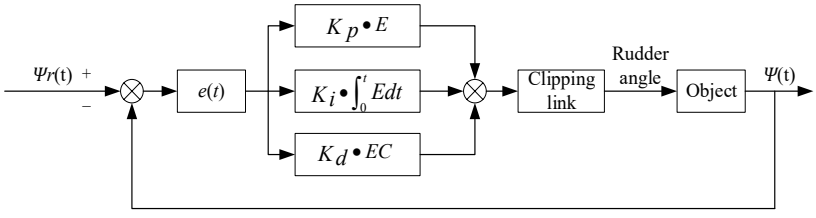

Fig. 6 A schematic diagram of the PID course autopilot

Its control law is shown in equation (2):

$$\delta(t) = K_p\left[e(t) + \frac{1}{T_i}\int_0^t e(t)\,dt + \frac{T_d\,de(t)}{dt}\right] \tag{2}$$

For computer simulations, discretisation of the integral and differential terms in equation (2) is necessary. Here, a sequence of sampling time points kT_p (where k denotes the sampling sequence number, and T_p is the sampling period) replaces the continuous time t. The integral is approximated using summation, and the differential is approximated using increments. This transformation yields equation (3), as detailed in [19]:

$$\begin{cases} t \approx kT_p \quad (k = 1, 2, 3\ldots) \\ \int_0^t e(t)dt = T_p \sum_{j=0}^{k} e(jt) = T_p \sum_{j=0}^{k} e(j) \\ \dfrac{de(t)}{dt} = \dfrac{e(kT_p) - e\left[(k-1)T_p\right]}{T_p} = \\ \dfrac{e(k) - e(k-1)}{T_p} \end{cases} \tag{3}$$

To ensure control accuracy within a short period, it is essential to simplify $e(kT_p)$ in equation (3) to $e(k)$. This simplification facilitates the derivation of a discrete PID expression, as shown in equation (4), by substituting equation (3) into equation (2):

$$\delta(k)=e(k) + K_i \sum_{j=0}^{k} e(j) + K_d \left[e(k) - e(k-1)\right] \tag{4}$$

Equation (4) defines $\delta(k)$ as the rudder angle control value at time k, and $e(k)$ as the course deviation at the same time instance. The integral coefficient K_i is determined by K_p, Δt, and T_i, while the differential coefficient K_d is derived from K_p, T_d, and Δt. Due to the full output mode, the controller's historical values are crucial for each output. In the case of position sensor failure, the rudder angle control output may undergo significant adjustments, leading to amplified steering amplitudes. To address these shortcomings, the positional PID control algorithm was optimised by introducing an incremental PID control algorithm.

Equation (5) is obtained by recursion of equation (4):

$$\delta(k-1)=e(k-1) + K_i \sum_{j=0}^{k-1} e(j) + K_d \left[e(k-1) - e(k-2)\right] \tag{5}$$

By subtracting equation (5) from equation (4), the incremental PID control algorithm expression shown in equation (6) can be obtained:

$$\Delta\delta(k)=K_p \Delta e(k) + K_i e(k) + K_d \left[\Delta e(k) - \Delta e(k-1)\right] \tag{6}$$

Equation (6) shows that the primary parameters influencing the rudder angle output are K_p, K_i, and K_d. Traditionally, ship operators have relied on their experience to set these parameters, leading to subjective and random adjustments. However, when factors such as load, speed, draft variations, and strong external interferences occur, achieving timely and precise adjustments is challenging.

3.2 Design of a PID course control system based on an optimal control strategy

An optimal control algorithm is proposed to enhance the accuracy of the ship's course, reduce fuel consumption, expedite reaching the destination, and optimise the sailing process. This strategy dynamically adjusts the PID parameters based on the ship's actual course, fuel consumption, and sailing conditions to ensure optimal sailing performance [20]. As illustrated in Fig. 7, the PID course control system architecture integrates this optimal control approach. Here, E represents the heading deviation, and EC signifies the deviation change rate.

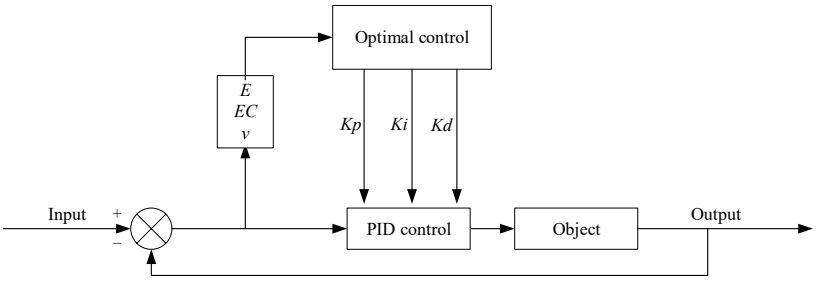

Fig. 7 A schematic diagram of an optimal PID

When ships sail, maintaining course accuracy and conserving energy are paramount concerns. While frequent course altering ensures precise heading control, it also escalates the power usage in the steering gear. To strike a balance between these factors across varying conditions, a quadratic performance index function was chosen, centred on both the course deviation and rudder angle control [20]:

$$J = \int_0^t \left(E^2 + \lambda \delta^2 \right) dt \tag{7}$$

In equation (7), E is the course deviation (Ψr-Ψ), δ is the rudder angle, λ is the weighting coefficient, λ values under different wind speeds are shown in table 2, and J is the comprehensive evaluation index.

Table 2 Correspondence table of λ values and wind speeds

Wind speed (m/s)	0~5	5~10	10~14	14~17	17~20	20~30	>30
λ	0.1	4	8	8.5	9	9.5	10

Optimal control yields the minimum value of the quadratic index function defined in equation (7). Utilising the output regulation theory of a linear-quadratic non-zero given point, the control law for the rudder angle was derived, as shown in equation (8):

$$\delta = \left[\frac{1}{\sqrt{\lambda}} \quad \frac{1}{K}\left(1 - \sqrt{1 + \frac{2KT}{\lambda}}\right) \right] \begin{bmatrix} E \\ EC \end{bmatrix} = \frac{1}{\sqrt{\lambda}} E + \frac{1}{K}\left(1 - \sqrt{1 + \frac{2KT}{\lambda}}\right) EC \tag{8}$$

where K and T are the cyclicity and followability indices, respectively, which can be obtained using equation (9):

$$\begin{cases} K = K' v / L \\ T = T' L / v \end{cases} \tag{9}$$

$$\begin{cases} K' = 47.875 - 2.64 \dfrac{L}{B} + 0.004 \dfrac{Ld}{A_R} + 66.589 C_b^2 - \\ \quad 112.702 C_b + 3.826 C_b \dfrac{L}{B} - 0.293 C_b \dfrac{B}{d} \\ T' = 26.464 + 0.408 C_b \dfrac{Ld}{A_R} - 0.033 \dfrac{L}{B} \dfrac{Ld}{A_R} - \\ \quad 79.114 C_b + 0.757 \dfrac{L}{B} + 46.129 C_b^2 \end{cases} \tag{10}$$

where L, B, and d are the length, ship width, and draft, respectively. C_b and A_R are the square coefficient and rudder area, respectively. K and T are directly and inversely proportional to the ship's longitudinal speed v, respectively.

The equations for calculating K_P and K_d are shown in equations (11) and (12):

$$K_P = \frac{1}{\sqrt{\lambda}} \tag{11}$$

$$K_d = \frac{1}{K}(1-\sqrt{1+\frac{2KT}{\lambda}}) \tag{12}$$

Ship course control, which functions as a closed-loop system, demonstrates second-order oscillations while maintaining asymptotic stability. The natural oscillation frequency and relative damping coefficient are estimated as follows:

$$\omega_n = \sqrt{\frac{K}{T\sqrt{\lambda}}} \tag{13}$$

$$\xi = \frac{1}{2}\sqrt{2+\frac{\sqrt{\lambda}}{KT}} \tag{14}$$

The control theory offers a method for determining the PID parameters through the second-order design approach outlined in equations (15)-(17):

$$K_P = \frac{T\omega_n^{\ 2}}{K} \tag{15}$$

$$K_i = \frac{\omega_n^{\ 3}}{10K} \tag{16}$$

$$K_d = \frac{2\xi\omega_n - 1}{K}T \tag{17}$$

In this method, ω_n represents the natural oscillation frequency, while ξ denotes the relative damping coefficient. It is crucial to constrain ξ within the range of [0.8, 1.0] to uphold system performance [21].

By substituting equations (13) and (14) into equations (15) and (17), respectively, K_P and K_d are derived. The obtained results align with equations (11) and (12). Consequently, K_i can be determined by substituting equations (13) into (16), as shown in equation (18):

$$K_i = \frac{1}{10}\sqrt{\frac{K}{T\lambda}} \tag{18}$$

Assuming the system course deviation parameters $e = \Psi - \Psi_r$, $\chi_1 = \Psi$, and $\chi_2 = \chi_1' = \Psi'$, the following equations can be used:

$$\begin{cases} \chi_1' = \chi_2 \\ \chi_2' = f(\chi_2) + bu \\ \psi = \chi_1 \end{cases} \tag{19}$$

where $b=K/T$, $u=\delta$, and $f(\chi_2)$ are represented by equation (20):

$$f(\chi_2) = -\frac{K}{T}H(\Psi') = -\frac{K}{T}(\alpha\Psi' + \beta\Psi'^3) \tag{20}$$

where β is the nonlinear factor coefficient, and K and T are ship manoeuvrability indices. The feedback controller was designed using a construction method, and a variable substitution was first made:

$$z_1 = e = \chi_1 - \psi_r \tag{21}$$

Assuming z_2 is the virtual control quantity, the following equation can be derived:

$$z_2 = \chi_2 - \phi(z_1) \tag{22}$$

where z_2 is the new state variable and z_1 is the stabilisation equation that makes z_1 approach zero equation (23):

$$\begin{cases} z_1' = \chi_1' - \psi_r' = \chi_2 - \psi_r' = z_2 + \phi(z_1) - \psi_r' = 0 \\ \phi(z_1) = \psi_r' - k_1 z_1 \end{cases} \tag{23}$$

where k_1 is the controller parameter, and $k_1>0$ equation (24) can be obtained from the above two equations:

$$z_1' = -k_1 z_1 + z_2 \tag{24}$$

Construct the first Lyapunov function $V_1=0.5z_1^2$, which is easy, to get equation (25):

$$V_1' = -k_1 z_1^2 + z_1 z_2 \tag{25}$$

At this time, if z_2 approaches 0, the above equation is a negative definite; that is, the z_1 and z_2 subsystems are calm.

Equation (26) is easy to obtain from equation (22):

$$z_2' = \chi_2' - \phi(z_1)' = f(\chi_2) + bu - \phi(z_1)' \tag{26}$$

We constructed the second Lyapunov function $V_2=V_1+0.5z_2^2$, which makes it easy to obtain equation (27):

$$V_2' = -k_1 z_1^2 + z_1 z_2 + z_2(f(\chi_2) + bu - \phi(z_1)') \tag{27}$$

To ensure that V_2 is less than or equal to zero, the following controller was designed:

$$u = \frac{1}{b}(\phi(z_1)' - z_1 - f(\chi_2) - k_2 z_2) \tag{28}$$

where k_2 is the controller parameter, and by substituting it into equation (27), it is easy to obtain equation (29), that is, V_2 is a negative definite:

$$V_2' = -k_1 z_1^2 - k_2 z_2^2 \tag{29}$$

That is, the use of a controller in equation (28) can stabilise the whole system, so that the system is asymptotically stable at $\chi_1=\psi_r$, $\chi_2=\psi_r'$.

3.3 Course control simulation experiment

To verify the course-control performance of the proposed controller, a conventional proportional-integral-derivative (PID) controller and an OP-PID controller were used for comparison and simulations, respectively. The simulation time was 550 s, the initial heading was 000°, the steering amplitude was 40°, and the traditional PID parameters set according to experience were $K_P = 1.61$, $K_i = 0.00078$, and $K_d = 9.75$. Ship speed $v = 5$ m/s and $\lambda = 0.1$. To make the simulation more consistent with practice, the characteristics of the servo system, namely, the rudder angle saturation limit, steering speed limit, and integral component, were considered. The maximum rudder angle was 35°, and the maximum steering speed was 2.7°/s. For

environmental interference, the direction and speed of the wind were 180° and 12 m/s, respectively, and the current speed was 1 m/s. The current direction in a fixed area does not fluctuate significantly for a period of time, and Python's random library randomly generates floating-point numbers within the range of [90°,120°] as the current direction. The simulation results are presented in Fig. 8.

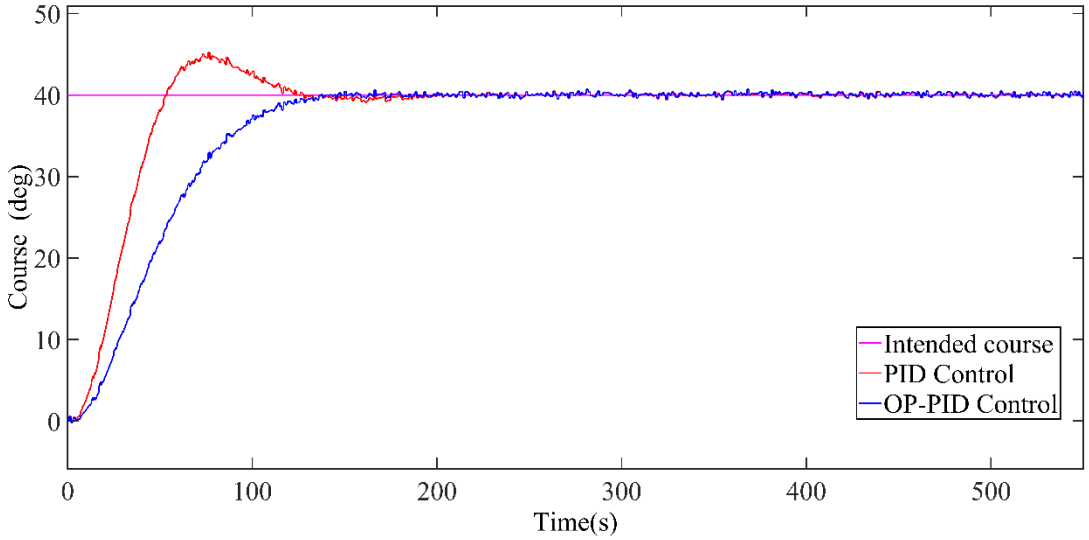

(a) Course control

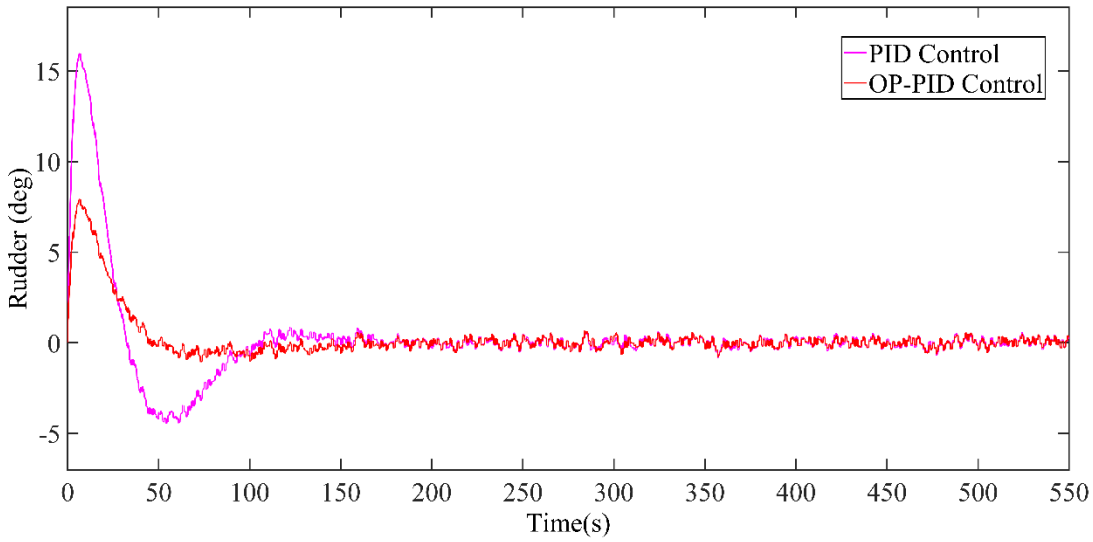

(b) Rudder angle control

Fig. 8 Comparison of the control effects

Table 3 Comparison of the control performance of the two control schemes

Control method	Course change E/(°)	Overshoot σ/%	Settling time ts/s	Maximum rudder angle δ/(°)
PID control	40	13.25%	240	16
OP-PID control	40	1.75%	175	7

As shown in Fig. 8 and Table 3, the OP-PID control has good stability, short response time, good dynamic response characteristics, and adaptability. The rudder angle amplitude of the OP-PID control is small, and the steering frequency is low, whereas the traditional PID control often uses a large rudder angle, which not only means more energy consumption and steering device wear, but may also cause the ship to capsize when the bending section and environmental interference are large, posing a threat to navigation safety. The course and rudder angle control performances of the control algorithm during variable-speed navigation in

curved channels were further analysed. The simulation time was 2500 s, and the initial speed v_1 was 5 m/s. At 1000 s, when the speed was changed to $v_1 = 3$ m/s. The two control algorithms were compared and tested, and the results are shown in Fig. 9.

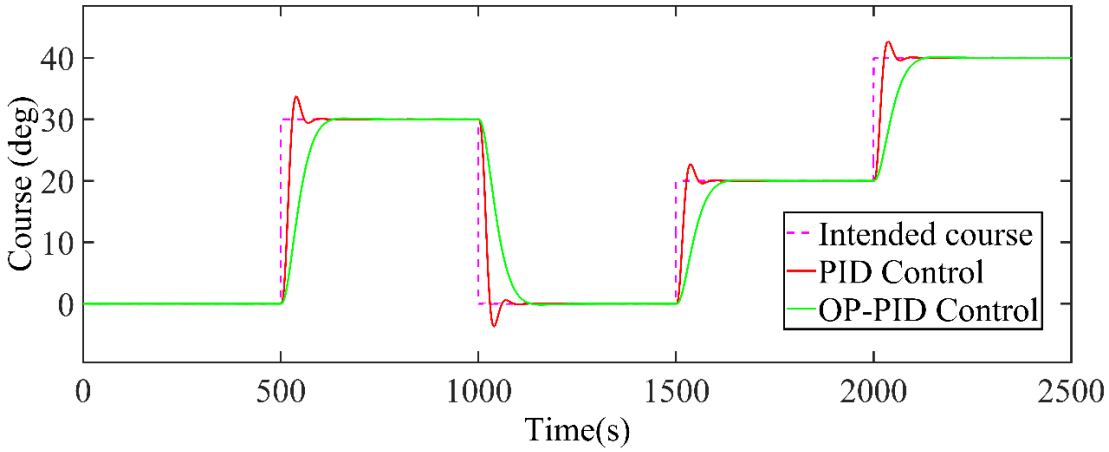

(a) Course control

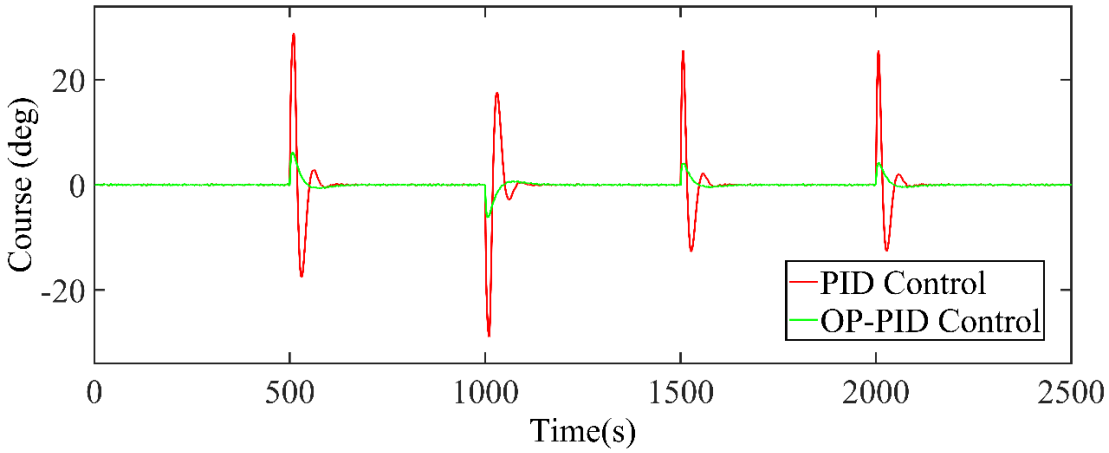

(b) Rudder angle control

Fig. 9 Comparison of the control effects

Table 4 Comparison of the control performance of the two control schemes (analysis from 0 to 800 s)

Control method	Course change E/(°)	Overshoot σ/%	Settling time ts/s	Maximum rudder angle δ/(°)
PID control	30	12.70%	600	27
OP-PID control	30	0.00%	730	6

As it can be seen from Fig. 9 and Table 4, the overshoot of the traditional PID was 12.7% at 0–800 s, while the OP-PID had almost no overshoot. As the target course changed, the PID controller oscillated and overshook. The OP-PID responds to course changes quickly, and the course curve is almost consistent with the target course. Compared with the PID control, the OP-PID control has higher precision and faster response speed. Analysis of the rudder angle control curve shows that the rudder angle amplitude of the OP-PID control is obviously small, and the PID control often uses a large rudder angle (e.g., steering 27° under 0–800 s PID control; steering 6° under OP-PID control). This not only means more energy consumption and steering device wear, but may also cause the ship to capsize when the bending section and environmental interference are large, posing a threat to navigation safety. When $v_1 = 5$ m/s, the course convergence time of the OP-PID control was less than that of the traditional PID control, and the traditional PID had an overshoot, indicating that the

OP-PID course controller is faster and has good stability. When the ship speed decreased from the original $v_1 = 5$ m/s to $v_2 = 3$ m/s at 1000 s, both the rudder angle output and the overshoot increased without changing the traditional PID parameters, indicating that the control effect of the traditional PID controller worsened when the ship speed changed. At the same time, the OP-PID course controller does not require manual tuning parameters and still has a good control effect when the speed changes, and its output response time and stability performance are obviously better than those of the traditional PID course controller; that is, the OP-PID course controller is not sensitive to speed changes and can better adapt to changes in ship speed.

4. Ship speed control method

4.1 The process of changing the ship's speed

The speed of the ship is adjusted by altering the propeller rotation rate, which is often communicated through a telegraph for speed commands. This adjustment involved two distinct processes: a rapid change in the propeller rotation rate and a slower change in the ship speed. Typically, the propeller rotation rate changes linearly, whereas the ship speed changes nonlinearly.

The telegraph and corresponding speed data of the simulation ship in Section 2.2 are shown in Table 5.

Table 5 Telegraph tachometer

Telegraph	Rotation（rpm）	Speed (kn)
Sea speed	93	14
Full ahead	85	12
Half ahead	70	10.5
Slow ahead	48	5
Dead slow ahead	35	3

When a telegraph command is issued at time t_1, the propeller rates before and after the speed change are denoted NP_1 and NP_2, respectively. t_2 denotes the moment at which the propeller rotation rate change is completed. The speed at time t is determined using equation (30):

$$NP^t = \begin{cases} NP_2, & t > t_2 \\ NP_1, & t < t_1 \\ NP_1 - (t - t_1) \times k, & t_1 < t < t_2 \text{ and } NP_1 > NP_2 \\ NP_1 + (t - t_1) \times k, & t_1 < t < t_2 \text{ and } NP_1 < NP_2 \end{cases} \tag{30}$$

The variable k represents the rate of change in the propeller rotation rate. Based on the insights gained from the simulation experiments and the expertise of the ship captain, it was determined that k equals two rotations per second.

Fig. 10 depicts the dynamics of ship speed and propeller rotation rate during deceleration from full ahead to half ahead. Notably, the propeller rotation rate experienced more rapid fluctuations than the gradual change in ship speed. Under fixed external conditions and target speeds, the distance covered by the ship during speed transition remained consistent. v_{d0} represents the ship speed at time t_{d0} when the telegraph command is initiated (considering deceleration as an example), and v_m signifies the target ship speed. At time t_1, the ship achieves the target speed. The area enclosed by the red-shaded portion on the left side of the graph represents the distance covered by the ship during this process. If the telegraph command is issued at time $t_{d0}+\Delta t$, it essentially implies a shift of Δt units to the right along the left curve. However, the area bounded by the speed and horizontal axes remains unchanged.

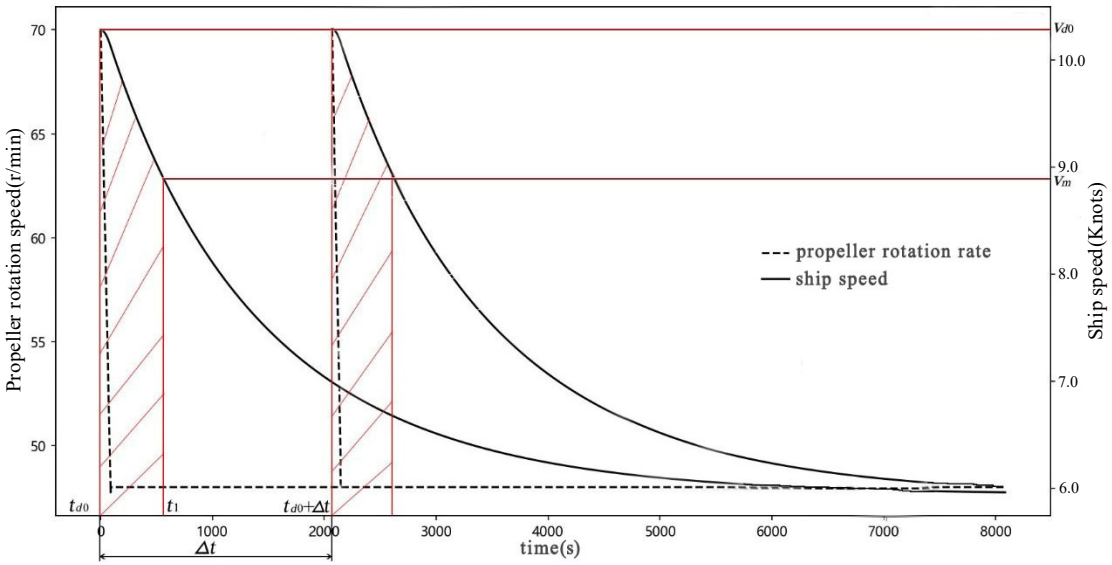

Fig. 10 The changes in ship speed and propeller rotation

4.2 Ship speed control method based on dichotomy

When navigating through curved channels, ships often engage in standby engine procedures involving engine reduction, stopping, or even reversal prior to entering the curve to mitigate speed. Additionally, upon approaching the curve, augmenting the propeller discharge flow enhances the ship responsiveness, thereby increasing the ship ratio and rudder efficiency. Consequently, preemptive speed adjustment at the control points is customary.

Assuming that the ship maintains a constant velocity v_{d0} and aims for a target speed v_m, with the telegraph issued at t_d, the ship speed reaches v_m at t_1 and the ship arrives at the control point at t_2. Ideally, the telegraph issuance time t_d aligns with t_{d0} to synchronise t_1 and t_2, ensuring t_2-t_1 = 0. The timing of the telegraph service issuance directly influences the distance (*dis*) required for the ship to reach the target speed from the current moment. Consequently, *dis* becomes a function of the telegraph issuance time t_d. If the ship maintains a constant speed v_{d0} and gives a telegraph order at t_d, then $dis(t_d)$ represents the distance from the present moment until the ship attains its target speed, as shown in equation (31):

$$dis(t_d)=\int_{t_d}^{t_2} v(t)dt=\int_{t_d}^{t_1} v(t)dt+\int_{t_1}^{t_2} v(t)dt=\lim_{n\to\infty}\sum_{i=1}^{n} v(t)[t_d+\frac{i}{n}(t_1-t_d)]\cdot\frac{t_1-t_d}{n}+\lim_{n\to\infty}\sum_{i=1}^{n} v(t)[t_1+\frac{i}{n}\cdot(t_2-t_1)]\frac{(t_2-t_1)}{n} \tag{31}$$

As it can be seen from equation (31), finding $t_d = t_{d0}$ satisfies the conditions and makes t_2-t_1 = 0; that is, finding $t_d = t_{d0}$ makes equation (32) valid:

$$\begin{cases} \int_{t_1}^{t_2} v(t)dt=0 \\ dis(t_d)=dis(t_{d0})=\int_{t_{d0}}^{t_1} v(t)dt=\lim_{n\to\infty}\sum_{i=1}^{n} v(t)[t_{d0}+\frac{i}{n}(t_1-t_{d0})]\cdot\frac{t_1-t_{d0}}{n} \end{cases} \tag{32}$$

The *dis* corresponding to the telegraph order at different time points is shown in equation (33):

$$\begin{cases} \int_{t_1}^{t_2} v(t)dt = 0 \\ dis(t_d) = dis(t_d^0) = \int_{t_d^0}^{t_1} v(t)dt = \\ \lim\limits_{n\to\infty} \sum\limits_{i=1}^{n} v(t)[t_d^0 + \dfrac{i}{n}(t_1 - t_d^0)] \cdot \dfrac{t_1 - t_d^0}{n} \end{cases} \tag{33}$$

where t_{d0} is the time point at which the requirements are met, and the telegraph command is issued at the time of t_{d0}, so that the ship speed when the ship reaches the control point is exactly the target speed, and t_1 and t_2 coincide. That is, $t_1 = t_2$, and equation (34) must be established:

$$\begin{cases} \int_{t_1}^{t_2} v(t)dt = 0 \\ dis(t_d) = \int_{t_{d0}}^{t_1} v(t)dt \end{cases} \tag{34}$$

Under this condition, the distance $dis(t_d)$ of the ship from the current moment to the target speed is the area of the curved trapezoid $abet_1t_m$ shown in Fig. 11, denoted as $dis(t_{d0})$.

When the time for giving the telegraph order is earlier than t_{d0}, equation (35) must be established. At this time, $t_1 < t_2$. That is, the ship has not reached the control point when it reaches the target speed. Fig. 11 shows that the distance $dis(t_d)$ is the area of the curved trapezoid $adt_{2m}t_m$ from the current moment to the target speed, which is smaller than the area of the curved trapezoid $abet_1t_m$:

$$\begin{cases} \int_{t_1}^{t_2} v(t)dt > 0 \\ dis(t_d) = \int_{t_d}^{t_{d0}} v(t)dt + \int_{t_{d0}}^{t_1} v(t)dt \end{cases} \tag{35}$$

When the time point for giving the telegraph order is later than t_{d0}, equation (25) must be established. At this time, $t_1 > t_2$; that is, the ship passes the control point when it reaches the target speed. Fig. 11 shows that the distance $dis(t_d)$ is the area of the curved trapezoid $acft_{2n}t_m$ from the current moment to the target speed, which is significantly larger than the area of the curved trapezoid $abet_1t_m$.

$$\begin{cases} \int_{t_1}^{t_2} v(t)dt < 0 \\ dis(t_d) = \int_{t_{d0}}^{t_d} v(t)dt + \int_{t_{d0}}^{t_2} v(t)dt + \int_{t_2}^{t_1} v(t)dt \end{cases} \tag{36}$$

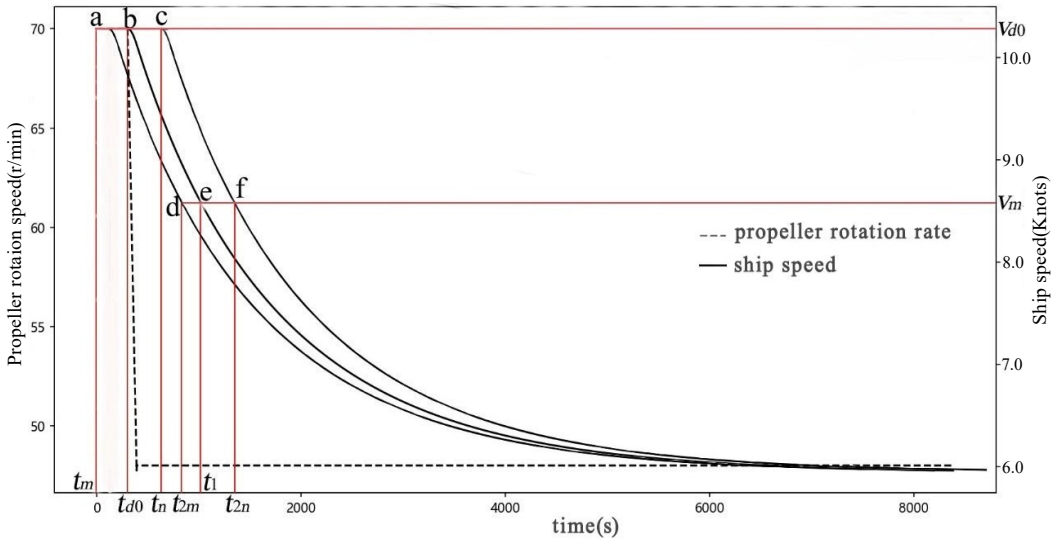

Fig. 11 Mapping diagram of *dis-t*

Equation (32) poses a challenge for traditional mathematical methods owing to its integral nature, compounded by the unknown integrand function $v(t)$. To address this complexity, a dichotomy method is proposed to iteratively approximate the numerical solution of telegraph order timing using deceleration as an illustrative example. The detailed solution procedure is shown in Fig. 12. In Fig. 12, NP_j (where j = 1, 2, 3, 4, and 5) denotes the propeller rotation rate corresponding to the five telegraph positions of the engine, and t_{Pi} represents the time point when the ship reaches the position point P_i. P_1 and P_2 denote the initial and target position points, respectively. v_1 and v_m denote the initial and target speeds, whereas the parameters Δv and Δd denote the speed threshold and distance threshold, respectively.

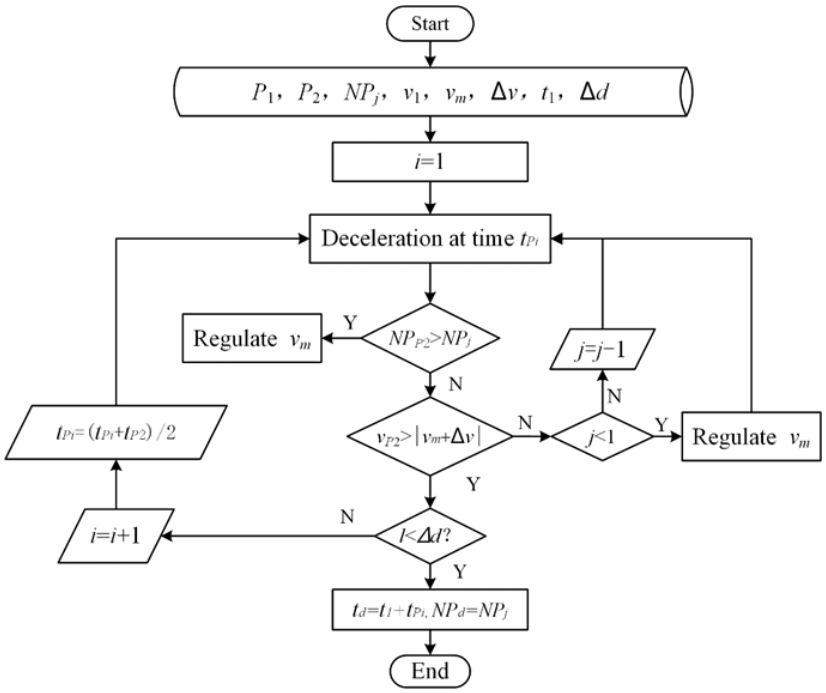

Fig. 12 A schematic diagram of speed control.

5. Ship tracking and speed control method and simulation of a curved section

5.1 Method of segment identification

A curved channel typically comprises multiple segments. The purpose of the segment identification method is to determine the current segment of a ship based on its current position, the boundary of the channel, planned route, and other information. Segment identification is the basis for the guidance algorithm to calculate the target course, and its principle is illustrated in Fig. 13.

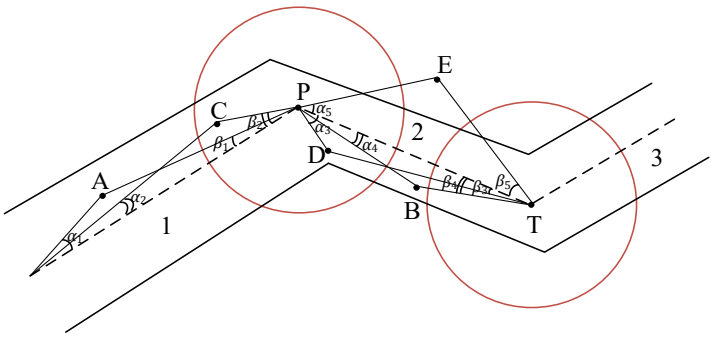

Fig. 13 Ship and route position relation in the segment identification method

In Fig. 13, the solid black line is the channel boundary, the dashed black line is the planned route, P and T are the waypoints on the planned course, the red area is the circle with the waypoint as the centre, and the radius of the advance turning distance R, A, B, C, D, or E is the ship's position at a certain time, and 1, 2, and 3 represent the segment numbers.

When the ship is at point A, it connects point A to the endpoint of the planned route for each segment. By analysing the angle of the connection between point A and the end points of the planned route and the planned route, it was found that only the two angles α_1 and β_1 of the planned route of Segment 1 are less than or equal to 90°, while the angle between the planned route of other segments is an obtuse angle and the ship belongs to Segment 1. The distance of the line segment AP is greater than the advance turning radius R, and the ship still takes the planned route of Segment 1 as the tracking control target. When the ship is at point C, point C is connected to the endpoints of the planned route of each segment. By analysing the angle of the connection between point C and the end points of the planned route and the planned route, it was found that only the two angles α_2 and β_2 of the planned route of Segment 1 are less than or equal to 90°, while the angle between the planned route of other segments is an obtuse angle and the ship belongs to Segment 1. The distance of the line segment CP was less than the advance turning radius R, and the ship used the planned route of Segment 2 as the tracking control target. When the ship is at points B and D, it is not difficult to determine whether it belongs to Segment 2 using the above method. When the ship is at point E, although outside the channel boundary, it can also be identified by using the above method. By connecting point E with the endpoints of the planned routes of each segment, and analysing the angle of the connection between point E and the end points of the planned routes and the planned routes, it was found that only the two angle α_5 and β_5 of the planned routes of Segment 2 are less than or equal to 90°, while the angle between the planned routes of other segments is an obtuse angle and then the ship belongs to Segment 2. The distance of the line segment ET is greater than the advance turning radius R, and the ship still takes the planned route of Segment 2 as the tracking control target.

The above segment identification method can be expressed using the flowchart shown in Fig. 14.

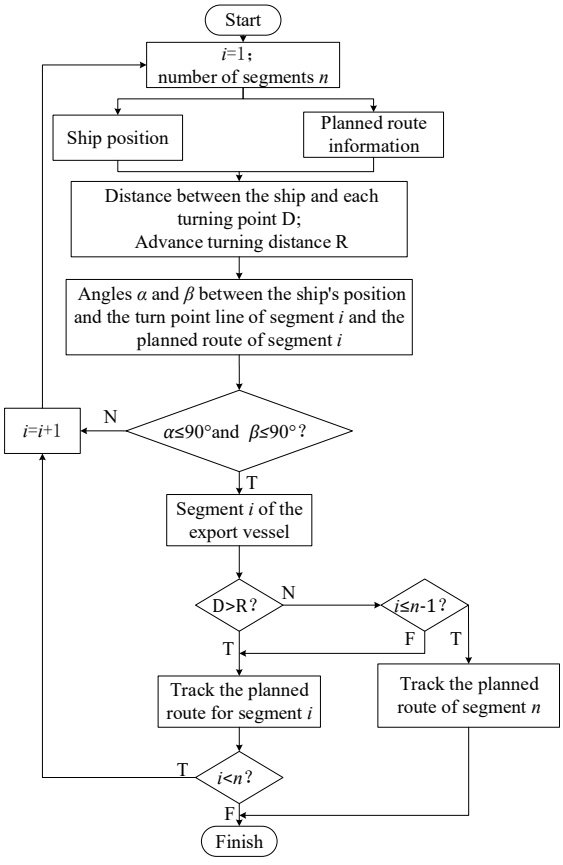

Fig. 14 Segment identification flow chart

5.2 Improved line-of-sight (LOS) guidance method

In practice, the planned route is obtained by connecting a straight segment to a waypoint. When the ship is at an appropriate distance from the next waypoint, the crew members control the ship to turn ahead and track its next leg. To improve the dynamic and static performance of track control systems, LOS guidance is improved. Fig. 15 illustrates the principles of conventional LOS guidance.

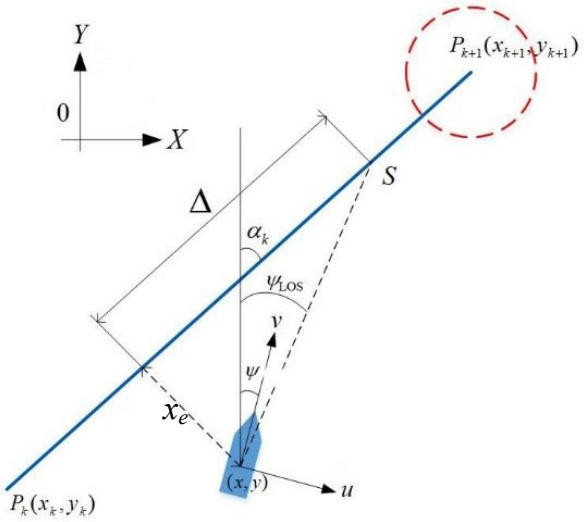

Fig. 15 Schematic diagram of LOS guidance

If the direction of the target segment is known when the ship is sailing at any position, track deviation can be calculated using a coordinate transformation:

$$x_e = -\cos\alpha_k (x - x_k) + \sin\alpha_k (y - y_k) \tag{37}$$

In equation (37), α_k is the angle between the north direction of the geodetic coordinate system and the planned track segment P_kP_{k+1}, which is called the track direction, (x_k, y_k) is the coordinate of the waypoint P_k, and (x, y) is the coordinate of the ship's current position. When the ship is on the right side of the planned route, $x_e > 0$. When the left side of the course is planned, $x_e < 0$. Thus, the LOS angle based on the forward-looking distance can be expressed by equation (38):

$$\begin{cases} x_e < 0, \quad \psi_{\text{LOS}} = \alpha_k + \arctan(\dfrac{-x_e}{\Delta}) \\ x_e > 0, \quad \psi_{\text{LOS}} = \pi - \left(\alpha_k + \arctan(\dfrac{x_e}{\Delta}) \right) \end{cases} \tag{38}$$

If $\Psi_{\text{LOS}} < 0$, then $\Psi_{\text{LOS}} = \Psi_{\text{LOS}} + 2\pi$. Δ is the forward-looking distance; that is, the distance between the projected point of the ship's current position on the target segment and point S. Arctan $(-x_e/\Delta)$ ensures that ship speed is a point pointing to the planned segment, which is located a point in the $\Delta > 0$ position.

Assuming the heading deviation is Ψ_e, equation (39) is given as:

$$\psi_e = \psi_{\text{LOS}} - \psi \tag{39}$$

The ship's turning amplitude is located at $[-\pi, \pi)$, " − "and " + "represent portside and starboard, respectively. Then, equation (40) is given as:

$$\begin{cases} -2\pi < \psi_e < -\pi, \quad \psi_e = \psi_e + 2\pi \\ \pi < \psi_e < 2\pi, \quad \psi_e = \psi_e - 2\pi \end{cases} \tag{40}$$

When $\Psi_e \rightarrow 0$, the ship sails towards the target point P, reaches the planned route, and completes the track tracking. According to the control algorithm, the current course angle Ψ is followed by the expected course angle Ψ_{LOS}, and the ship can sail along the planned section. As a ship travels along a segment, it is necessary to determine whether to alter its course to track the next segment. In the conventional LOS guidance method, equation (41) is generally used as a criterion to directly track the waypoint of the ship. However, in actual sailing, owing to the influence of external interference such as wind and currents, it is difficult for the ship to accurately reach the waypoint. Suppose there is a circle with waypoint $P_{k+1}(x_{k+1}, y_{k+1})$ as the centre and R as the radius, the ship's current position $P(x, y)$ satisfies the following conditions:

$$(x_{k+1} - x)^2 + (y_{k+1} - y)^2 \leq \mathrm{R}^2 \tag{41}$$

This indicates that the ship's tracking is completed in this segment and begins to track the next segment; that is, when the distance between the ship and the next waypoint is less than the given advance distance R, the autopilot begins to turn.

In order to solve the problem that LOS guidance method cannot eliminate static track errors under wind and current interference, and the dynamic characteristics are not ideal due to the unchanged forward looking distance Δ and advance turn R, the LOS guidance method is improved in two aspects. In the traditional LOS guidance method, the forward looking distance Δ is generally 3–5 times the length of the ship. It can be seen from equation (38) that the reciprocal of the LOS angle based on the forward-looking distance is equivalent to a coefficient proportional to x_e. This is similar to the concept of fuzzy control: if it can be updated using the error value, the transient performance will be improved.

A time-varying forward looking distance Δx_e is proposed in equation (42):

$$\Delta(y_e) = (\Delta_{\max} - \Delta_{\min}) e^{-r|y_e|} + \Delta_{\min} \tag{42}$$

In equation (42), $\Delta_{\max}$ and $\Delta_{\min}$ are the maximum and minimum values of Δ, respectively, and r is the convergence rate. When the ship is far from the planned route and x_e is large, Δ is small, and the convergence rate is increased to speed up the convergence of the track deviation. When the ship approaches the planned route and needs to avoid deviation, x_e is smaller and Δ is larger, reducing the convergence rate to prevent the ship from swinging on both sides of the planned route. Limiting factors such as ship manoeuvring characteristics should be taken into account when determining $\Delta_{\max}$, $\Delta_{\min}$, and the convergence rate r.

The advance distance R set during segment switching has a significant influence on track error and steering; therefore, R should be set reasonably. In order to stabilise the transition between track segments when sailing in open waters, relatively large track errors can be allowed; therefore, a larger value of R is desirable [22]. However, when sailing in the water of a bridge, the heading is strongly restricted by the bridge width. To avoid collisions, a large track error is not allowed when the track section is switched. Therefore, R should have a smaller value. R is usually 2 times the length between the perpendiculars of the ship. Conventional LOS guidance requires the ship to turn ahead at a fixed distance from the waypoint (e.g., two times the ship's length) [23]. This strategy was acceptable for small turning angles. However, if the advanced steering distance is insufficient in the case of large angles, the ship will deviate by a large distance at the turn. After many experiments, a new strategy equation based on the rudder angle and ship length was proposed to improve the performance of the guidance method.

$$\mathrm{R} = (3\theta_{turn} + 1.5)L \tag{43}$$

In equation (43), θ_{turn} and L are the rudder angle and ship's length, respectively, and the rudder angle is converted by the arc length formula. With the new advanced turning distance, a sufficient turning distance can be maintained when the turning angle is sufficiently large.

5.3 Calculation of track deviation

In equation (38), when the ship is sailing at any position, assuming that the direction of the target segment is known, the track deviation can be calculated using coordinate transformation. In this case, the

angle α_k between the geodetic coordinate system and the planned segment P_kP_k+1 needs to be known. Based on this method, a track deviation triangle is established to obtain the track deviation:

$$y_e = \frac{\left|x\left(y_k - y_{k+1}\right) + y\left(x_{k+1} - x_k\right) + \left(x_k y_{k+1} - x_{k+1} y_k\right)\right|}{\sqrt{\left(x_{k+1} - x_k\right)^2 + \left(y_k - y_{k+1}\right)^2}} \tag{44}$$

In equation (44), (x, y) is the current position coordinate of the ship, (x_k, y_k) is the starting coordinate of the target segment, and (x_{k+1}, y_{k+1}) is the end coordinate of the target segment.

5.4 Ship track and speed control method based on model prediction and feedback compensation

Track control error mainly originates from three aspects: situational awareness error, ship manoeuvring motion model parameter error, and control parameter error. Improving the sensor accuracy and optimising the model and control parameters can reduce the deterministic errors. In addition, feedback adjustment based on closed-loop inputs compensates for the nondeterministic errors.

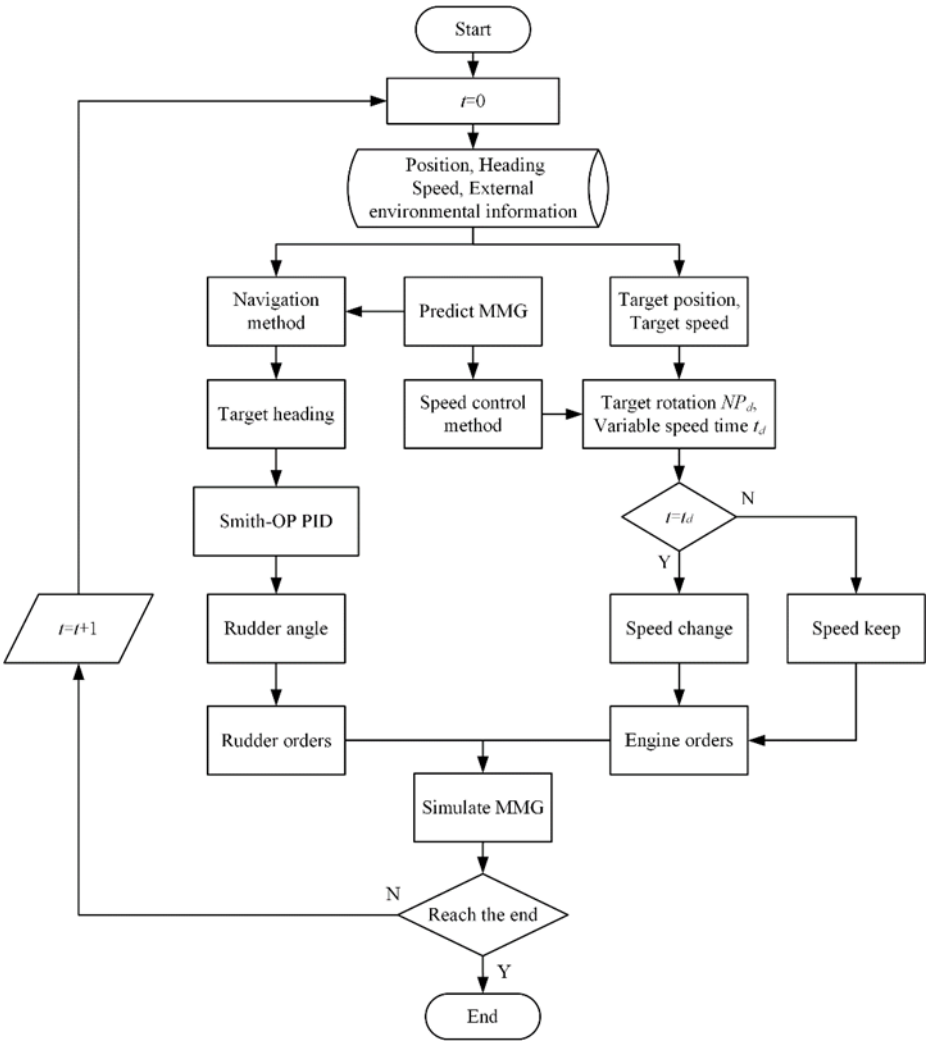

Fig. 16 A schematic diagram of track and speed control.

In view of the dynamic characteristics of environmental interference in actual navigation, to reduce errors and achieve accurate track control, an adaptive closed-loop track control method is proposed in this paper to deal with the interference effect of complex dynamic environments on ship manoeuvring. This method consists of three key modules: situational awareness, scheme decision and execution, and iteration to form a closed loop. It consists of the following steps: (1) the situational awareness module obtains the ship status and environment information to provide input for subsequent decisions; (2) the solution decision module

deeply couples the front-end situational awareness result and the back-end execution process and makes the heading speed decision according to the environmental judgment and execution inference; (3) the executive module controls the steering gear and propulsion system to complete the operation; (4) the above steps are repeated, using the feedback from each execution to adjust the decision.

Specifically, the obtained ship and environmental information were input, and the control execution plan was generated as an output through the prediction, decision, and execution modules. During the execution process, the feedback course and speed deviation were measured and the control scheme was adjusted to achieve a real-time response to environmental changes. The simplified MMG model used in the prediction module ignores environmental interference factors, whereas the MMG model of the simulation module includes the disturbances of wind, waves, and currents. After Δt time, the MMG model of the simulation module is controlled according to the decision scheme of the ship position, speed, and other output information of the prediction MMG model, so as to achieve real-time feedback adjustment and gradually reduce the nondeterministic error. Fig. 16 illustrates this process.

5.5 Track and speed control simulation

5.5.1 Research waters

The Dongboliao Channel is located west of Hong Kong Island, and the navigation rules of this area stipulate that inbound and outbound vessels sail within the corresponding navigable lanes; that is, the water area can be divided into inbound and outbound channels. The outbound channel is narrower and more continuously curved than the inbound channel, and the narrowest point is approximately 0.25 nautical miles. Therefore, the outbound channel of the Dongboliao Channel was considered as the research water area. The outbound channel can be divided into five sections from north to south, and its latitude and longitude ranges are 22°7.801 N–22°19.825 N and 114°7.559 E to 114°20.248 E, as shown in Fig. 17.

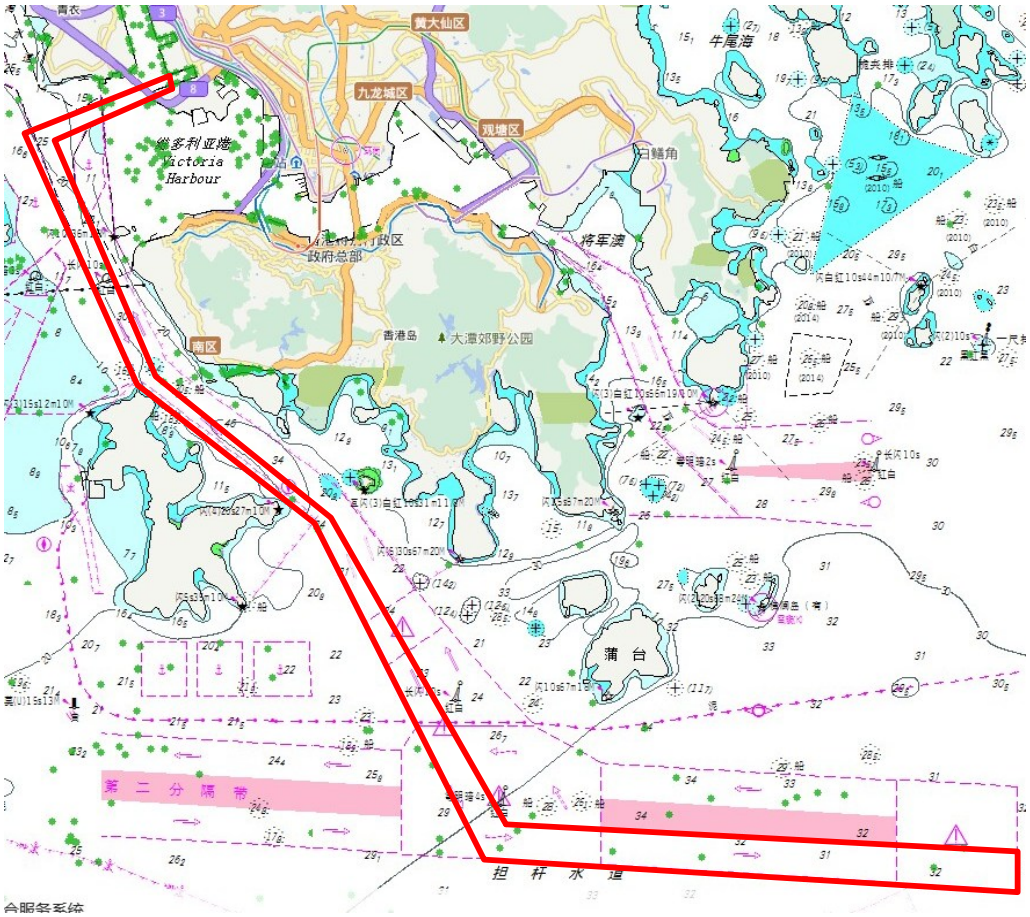

Fig. 17 Research waters

Under normal circumstances, ships should not cross or enter a separation zone when they sail in a traffic separation zone. Therefore, the boundary of the traffic separation zone was considered as the channel boundary, and the centreline of the channel was set as the planned route. The environmental disturbance is reflected by the interference force and torque in the MMG model in Section 1.2, and the digital traffic environment of the outbound channel of the Dongboliao Channel is constructed, as shown in Fig. 18.

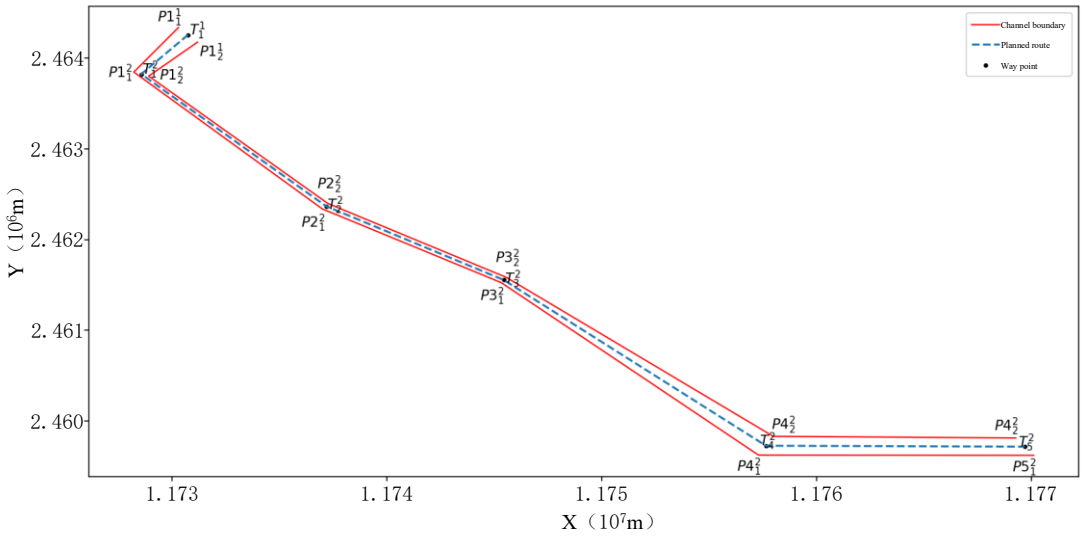

Fig. 18 Digital traffic environment of the exit channel of the Dongbaoliao Channel

As shown in Fig. 18, the Dongbaoliao Channel is divided into five segments (numbered 1 to 5 from north to south). Each segment contains two boundary lines (numbered from west to east). Each boundary line contains two endpoints, and the boundary lines of adjacent segments share one endpoint. Pi_a^b represents the b_{th} end point of the side a_{th} of segment i. The midpoint of the line between the end points of each segment boundary line is set as the waypoint, where the adjacent segments share a waypoint. T_m^n represents the n_{th} waypoint of the m_{th} segment, and the connection of each waypoint is the planned route. L_i represents the planned route within the i segment. The relative position relationship of the channel boundary line, planned route, and waypoint can be expressed by equations (45) and (46):

$$\begin{cases} T_m^n = P\left(\dfrac{Pm_1^n + Pm_2^n}{2}\right) \\ m = 1,2,3,4,5 \\ n = 1,2 \end{cases} \tag{45}$$

$$L_i = \begin{cases} l(T_i^1, T_i^2) & i = 1 \\ l(T_{i-1}^2, T_i^2) & i = 2,3,4,5 \end{cases} \tag{46}$$

where P and 1 represent the coordinate points and the line of the coordinate points, respectively.

5.5.2 Still water simulation

The initial position of the ship was (114.1263° N, 22.32965° E), whereas the initial course was 225°, the ship speed was 5kn, and the propeller rotation rate was 48 rpm. The target ship speeds of waypoints T_1^2, T_2^2, T_3^2, and T_4^2 were set to 2, 7, 5, and 6 kn, respectively, and the target ship speeds of the midpoint of points T_1^2 and T_2^2, T_2^2 and T_3^2, and T_3^2 and T_4^2 were set to 8, 8, and 7 kn, respectively. The track and speed control method composed of OP-PID, improved LOS guidance, and dichotom-based speed control (herein after referred to as Scheme 1) was compared and simulated with the track and speed control method composed of PID, LOS guidance, and dichotom-based speed control (hereinafter referred to as Scheme 2). The simulation results are presented in Fig. 19.

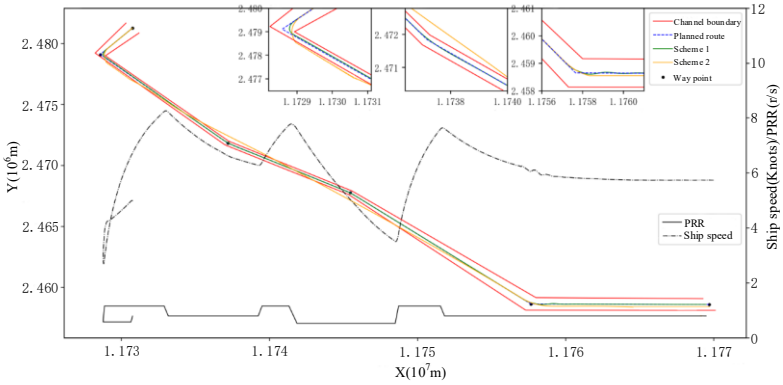

(a) Tracking and speed curves

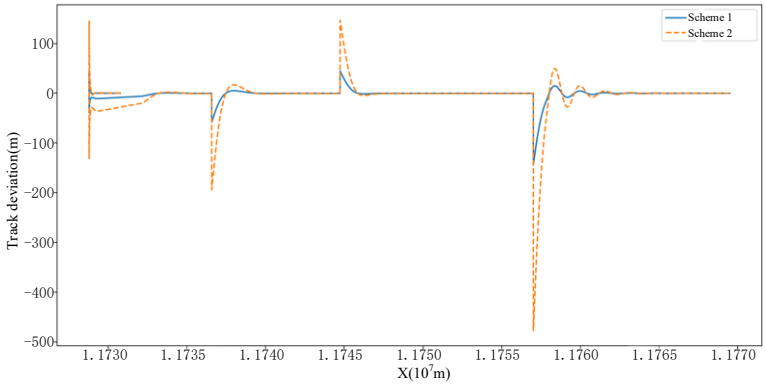

(b) Track deviation curve

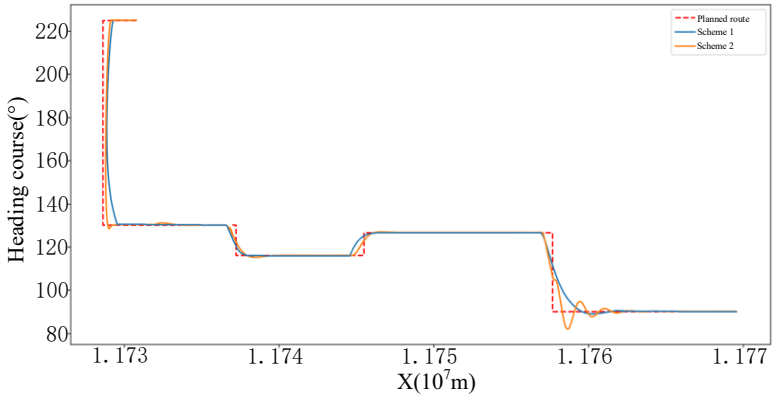

(c) Heading curve

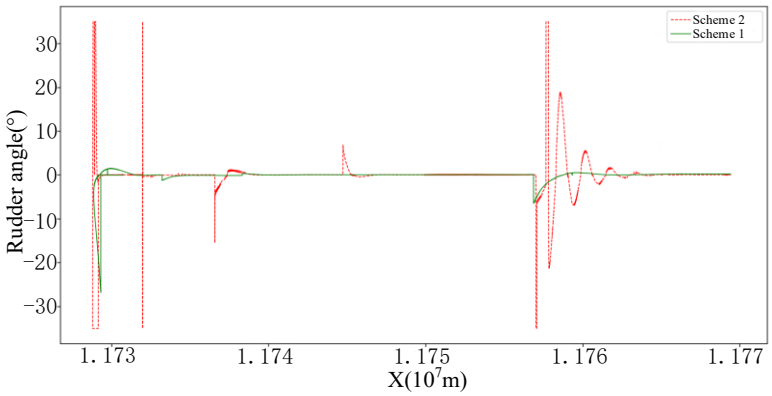

(d) Rudder angle curve

Fig. 19 Still water simulation

In Fig. 19(a), PRR represents the propeller rotation rate. When the ship is sailing from Segment 1 to Segment 2, under the control of Scheme 1, the ship can still smoothly enter Segment 2 from Segment 1, even if the curvature radius of the waypoint is small. Under option 2, the ship was already outside the channel boundary. At the waypoints of the remaining segments, the track curve under Scheme 1 was smoother and more consistent with the planned route than that under Scheme 2. In terms of speed control, the actual ship speed of the way points T_1^2, T_2^2, T_3^2, and T_4^2 are 2.29, 6.8, 5.06, and 6.14 kn and the target ship speed of the midpoint of the points T_1^2 and T_2^2, T_2^2 and T_3^2, and T_3^2 and T_4^2 are 8.24, 7.84, and7.28 kn, respectively, with a very small difference between actual ship speed and the target ship speed. The goal of accurately controlling the speed of the ship was achieved.

Fig. 19(b) shows the trajectory deviation curve calculated using equation (44). Evidently, the track deviation under Scheme 1 was smaller than that under Scheme 2, and the former converged faster than the latter. In Fig. 19(c), the heading of the ship under Scheme 1 approaches the target heading faster than that under Scheme 2, and the heading overshoot, the oscillation amplitude, and the frequency of the former are significantly lower than those of the latter. In Fig. 19(d), under the control of Scheme 1, the ship can stabilise its heading at a small rudder angle. Even if a large rudder angle is occasionally operated, the duration of the large rudder angle is shorter than that in Scheme 2. The amplitude, frequency, overshoot, and convergence time of the rudder angle under Scheme 1 were smaller than those under Scheme 2.

5.5.3 Simulation under environmental interference

The initial position of the ship was (114.1263° N, 22.32965° E), the initial heading was 225°, the speed of the ship was 5 kn, the propeller rotation rate was 48 rpm, the wind direction and wind speed were 180° and 12 m/s, the absolute wave direction angle was 180°, and the wave amplitude and velocity were 3 m and 1 m/s, respectively. Because the current direction in a fixed region does not fluctuate significantly over time, floating-point numbers randomly generated by Python's random library in the range [90,120] were used as the current direction. The target ship speeds of waypoints T_1^2, T_2^2, T_3^2, and T_4^2 were set to 2, 7, 5, and 6 kn and the target ship speeds of the midpoints of points T_1^2 and T_2^2, T_2^2 and T_3^2, and T_3^2 and T_4^2 were set to 8, 8, and 7 kn, respectively. The track and speed control method composed of OP-PID, improved LOS guidance, and dichotom-based speed control (hereinafter referred to as Scheme 1) was compared and simulated with the track and speed control method composed of PID, LOS guidance, and dichotom-based speed control (hereinafter referred to as Scheme 2). The simulation results are presented in Fig. 20.

In Fig. 20(a), under a changing current field, the track under the control of Scheme 2 exceeds the channel boundary at the waypoints of the three segments, whereas the track under the control of Scheme 1 remains within the channel boundary. Even if the radius of curvature of the channel is small, a ship can stably track and sail along the planned route. In terms of speed control, the actual ship speed of the way points T_1^2, T_2^2, T_3^2, and T_4^2 are 2.26, 6.77, 4.97, and 6.08 kn and the target ship speed of the points T_1^2 and T_2^2, T_2^2 and T_3^2, and T_3^2 and T_4^2 are 8.13, 7.79, and 7.14 kn, respectively. The speed deviation is kept within the controllable range. The goal of accurately controlling the speed was achieved.

Fig. 20(b) shows the trajectory deviation curve calculated using equation (44). Under a changing current field, the oscillation amplitude of the track deviation of the two schemes is significantly increased; however, the track deviation under Scheme 1 is still smaller than that under Scheme 2. Although both exhibit a certain degree of oscillation, the oscillation amplitude and frequency of the former are smaller and converge faster than those of the latter.

In Fig. 20(c), owing to the interference of the random current field, the ship's heading under both control schemes has a certain fluctuation near the target heading. However, in general, the fluctuation amplitude and frequency of Scheme 1 are smaller, and the ship's heading under Scheme 1 converges to the target heading faster than that under Scheme 2.

As shown in Fig. 20(d), to suppress environmental interference, the rudder angle curves of the two schemes show obvious oscillations. However, in comparison, the rudder angle under the control of Scheme 1 is smaller and the duration of the large rudder angle is shorter than that under Scheme 2. Although oscillation occurred, the amplitude, frequency, overshoot, and convergence time of the rudder angle under Scheme 1 were smaller than those under Scheme 2.

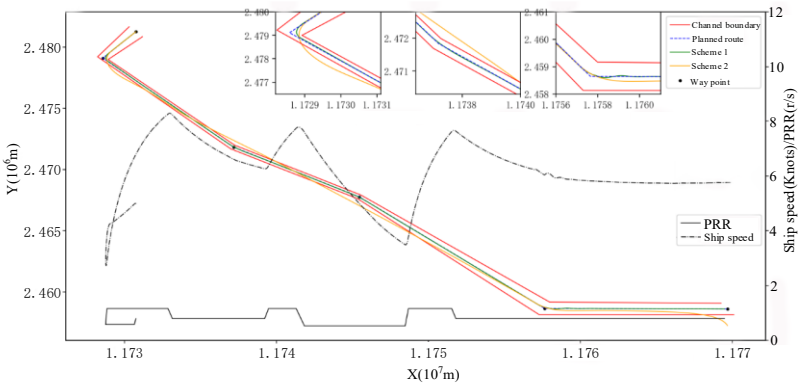

(a) Tracking and speed curves

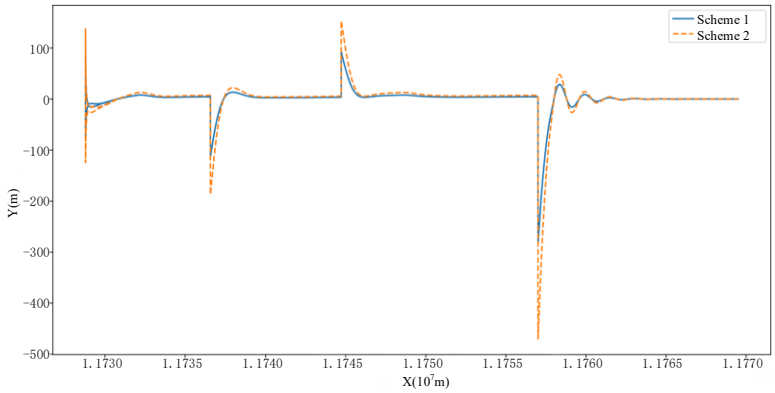

(b) Track deviation curve

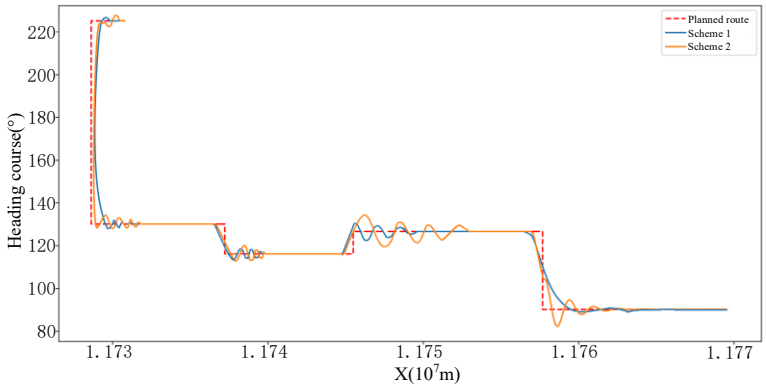

(c) Heading curve

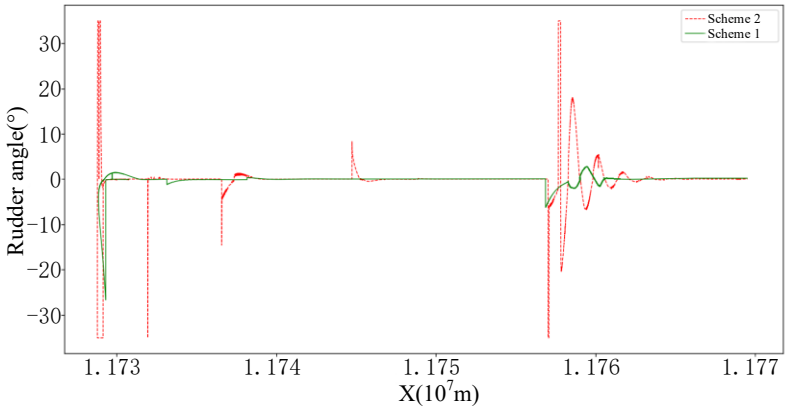

(d) Rudder angle curve

Fig. 20 Simulation under environmental interference

6. Conclusion and future prospects

Existing course and track control methods have difficulties in terms of adapting to the frequent course-altering operation of ships in curved channels, and ship speed control methods in curved channels that conform to navigation practice are still lacking. The following work was carried out in this study:

(1) First, the optimal control strategy was combined with the PID to design a heading controller that can adapt to the frequent course and speed alterations of curved channels and complex natural environments.

(2) Considering the practical practice of first decelerating and then accelerating when ships pass through a curved channel, the scientific principle of the ship speed shifting process was analysed, and a ship speed control method based on dichotomy was proposed.

(3) Considering that some system errors cannot be eliminated when the theoretical model is used to control an actual ship, a closed-loop track and speed control method was designed based on the theory of model predictive control and feedback compensation to reduce the influence of system errors on the control effect.

However, it may be noted that there are some unresolved problems in this study. For example, in this study, external interference, such as due to wind, waves, and currents, is simplified, but in the actual situation the changes in wind direction and speed as well as direction and velocity of currents in curved sections are very complicated; therefore, it is necessary to study and establish an environmental interference model. The constructed track and speed control scheme is the result of relatively idealised preconditions, resulting in a control scheme containing many empirical parameters that are not determined by a standardised process or logical calculation method in actual use. These parameters are generally obtained manually by repeated attempts in simulation experiments for specific ship types and environments, and cannot be implemented on real ships. In other words, many parameters are not adaptive.

Acknowledgments

This study was supported by the National Natural Science Foundation of China (Grant number 52071249).

REFRENCES

[1] Hugan, Z., Xianku, Z., Tian, C., Renxiang, B., 2022. Active disturbance rejection control for ship path following with Euler method. *Ocean Engineering*, 247, 110516. https://doi.org/10.1016/j.oceaneng.2021.110516

[2] Yunbo, L., Zongyu, T., Jiaye, G., 2023. The effect of PID control scheme on the course-keeping of ship in oblique stern waves. *Brodogradnja*, 74(4), 155-178. https://doi.org/10.21278/brod74408

[3] Jaime, A. L., Álvaro, G., 2023. Robust Model Predictive Control Based on Active Disturbance Rejection Control for a Robotic Autonomous Underwater Vehicle. *Journal of Marine Science and Engineering*, 11(5), 929. https://doi.org/10.3390/jmse11050929

[4] Liu, W., Ye, H., Yang, X., 2023. Model-Free Adaptive Sliding Mode Control Method for Unmanned Surface Vehicle Course Control. *Journal of Marine Science and Engineering*, 11(10), 1904. https://doi.org/10.3390/jmse11101904

[5] Xiaoyang, L., Zhiquan, L., Zhenzhong, C., 2020. Nonlinear Adaptive Heading Control for an Uderactuated Surface Vessel with Constrained Input and Sideslip Angle Compensation. *Brodogradnja*, 71(3), 71-87. https://doi.org/10.21278/brod71305

[6] Guoshuai, L., Xianku, Z., Wenjun, Z., Zhenhuan, Z., 2023. Z-shaped navigation for surface ships in rough seas based on constraint MPC. *Ocean Engineering*, 281, 114970. https://doi.org/10.1016/j.oceaneng.2023.114970

[7] Xiaofei, Y., Xin, Y., Wei, L., Hui, Y., Zhaoping, D., Weibo, Z., 2022. An improved stanley guidance law for large curvature path following of unmanned surface vehicle. *Ocean Engineering*, 266, 112797. https://doi.org/10.1016/j.oceaneng.2022.112797

[8] Yixiong, H., Liling, L., Weixuan, H., 2021. Decision Method of Autonomous Collision Avoidance for Stand-on vessels in Open Waters. *Journal of Wuhan University of Technology (Transportation Science & Engineering)*, 45(05), 994-999.

[9] Ahmed, H. Y., Masoud, D., Kareem M. A., 2024. Neural Network-Based Adaptive PID Controller Design for Over-Frequency Control in Microgrid Using Honey Badger Algorithm. *IEEE Access*, 12, 27989-28005. https://doi.org/10.1109/ACCESS.2024.3367288

[10] Guoshuai, L., Xianku, Z., 2022. Research on the influence of wind, waves, and tidal current on ship turning ability based on Norrbin model. *Ocean Engineering*, 259, 111875. https://doi.org/10.1016/j.oceaneng.2022.111875

[11] Nguyen, H. Q., Tran, A. D., Nguyen, T. T., 2019. The Bilinear Model Predictive Method-Based Motion Control System of an Underactuated Ship with an Uncertain Model in the Disturbance. *Processes*, 7(7), 445. https://doi.org/10.3390/pr7070445

[12] Wei, L., Zhao, L., Mingyang, Z., Yanjie, W., 2022. Standard method of ship speed control in harbor water area. *Navigation of China*, 45, 1–7.

[13] Wogi, L., Ayana, T., Morawiec, M., Jąderko, A., 2022. A Comparative Study of Fuzzy SMC with Adaptive Fuzzy PID for

Sensorless Speed Control of Six-Phase Induction Motor. *Energies*, 15(21), 8183. https://doi.org/10.3390/en15218183

[14] Ailong, F., Jian Y., Liu, Y., Weiqin, L., Nikola, V., 2022. Joint optimisation for improving ship energy efficiency considering speed and trim control. *Transportation Research Part D: Transport and Environment*, 113, 103527. https://doi.org/10.1016/j.trd.2022.103527

[15] Yu, X., Shutao, Z., Yu, Y., Zhiyong, Q., 2018. Ship Maneuvering Performance Prediction Based on MMG Model. *IOP Conference Series: Materials Science and Engineering*, 452(4), 042046. https://doi.org/10.1088/1757-899X/452/4/042046

[16] Djahida, B., Omar, I., 2017. Impact of Some Geometrical Aspects on the Tandem Co-Rotating Propeller Hydrodynamic Characteristics. *Brodogradnja,* 68(1), 107-123. https://doi.org/10.21278/brod68107

[17] Jinlai, L., Liwen, H., Deqing, Y., Luping, X., Yixiong, H., 2024. The control method for ship tracking when navigating through narrow and curved sections. *Applied Ocean Research*, 145, 103943. https://doi.org/10.1016/j.apor.2024.103943

[18] Yixiong, H., Xiaohan, Z., Weixuan, H., 2020. Ship Dynamic Collision Avoidance Mechanism Based on Course Control System. *Journal of Southwest Jiaotong University*, 55(05), 988-993.

[19] Siwei, X., Yixiong, H., Liwen, H., 2021. A novel ship path following method in inland waterways based on adaptive feedforward PID control. *Maritime Technology and Research*, 3(4), 377-405. https://doi.org/10.33175/mtr.2021.252309

[20] Ratnoo, A., Ghose, D., 2009. State-Dependent Riccati-Equation-Based Guidance Law for Impact-Angle-Constrained Trajectories. *Journal of Guidance Control and Dynamics*, 32, 320-326. https://doi.org/10.2514/1.37876

[21] Boxu, M., Xianku, Z., 2021. Concise robust fuzzy nonlinear feedback track keeping control for ships using multi-technique improved LOS guidance. *Ocean Engineering*, 224, 108734. https://doi.org/10.1016/j.oceaneng.2021.108734

[22] Atyya, M., El-Bayoumi, G. M., Lotfy, M., 2024. Optimal tracking control for underactuated airship. *Journal of Engineering and Applied Science*, 71, 2. https://doi.org/10.1186/s44147-023-00324-3

[23] Fossen, T., 2002. Marine control systems: guidance, navigation and control of ships, rigs and underwater vehicles. *Marine Cybernetics*, Trondheim, Norway